Inorganic Chemistry Communications 100 (2019) 129–133

Contents lists available at ScienceDirect

Inorganic Chemistry Communications

journal homepage: www.elsevier.com/locate/inoche

Short communication

Two pyrene-based S-containing atropisomers: Different structures and different Ag^+-response behaviors of their monomer-excimer emission

Ying-ying Jin, Qi Fang*, Shi-qian Zhang, Zhi-qiang Liu

State Key Laboratory of Crystal Materials, Shandong University, Jinan 250100, China

GRAPHICAL ABSTRACT

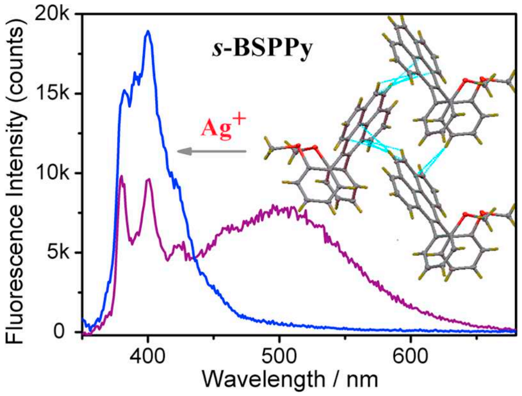

ARTICLE INFO

Keywords:
Pyrene compounds
Atropisomers
Crystal structures
Excimer emission
Ag^+-response

ABSTRACT

Different structures and different Ag^+-response behaviors of a pair of pyrene-based S-containing atropisomers, namely ***s*-BSPPy** and ***a*-BSPPy**, have been investigated. The calculated high rotation barrier indicates that the two atropisomers are non-interconvertible. In polar solvents, ***s*-BSPPy** exhibits excimer emission but ***a*-BSPPy** does not. Based on the X-ray structures and the DFT calculated intermolecular interactions, the excimer of ***s*-BSPPy** is suggested to take a non-parallel edge-to-face λ-shaped geometry. Especially, ***s*-BSPPy** exhibits ratiometric excimer-off and monomer-on emission as a unique response to Ag^+ in solutions, while no ratiometric Ag^+-response was observed for ***a*-BSPPy**.

Pyrene compounds are well-known polyaromatic organic species, which acquired wide applications for years [1–6]. The planar pyrene is an excellent fluorephore and the best-known example of excimer emission. The term excimer is an abbreviation for an excited-state dimer, which came into being soon after the early study of the broad long-wavelength emission of pyrene in concentrated solution [1]. Among various applications of excimer emission, the monomer-excimer switching properties of pyrene compounds can be used as sensitive ratiometric fluorescent chemosensors for metal ions [7–12] and anions [13–15].

The title two pyrene-based S-containing atropisomers are *syn*-4,5-bis(2-methylthio)phenyl-pyrene (***s*-BSPPy**) and *anti*-4,5-bis(2-methylthio)phenyl-pyrene (***a*-BSPPy**) (see Scheme 1), which have been briefly reported as the intermediates for synthesizing heterocycle-fused pyrene derivatives in the recent work of our group [6]. Atropisomers, commonly known as stable rotamers, are a family of stereoisomers that

---

* Corresponding author.
E-mail address: fangqi@sdu.edu.cn (Q. Fang).

https://doi.org/10.1016/j.inoche.2018.12.021
Received 10 December 2018; Received in revised form 25 December 2018; Accepted 27 December 2018

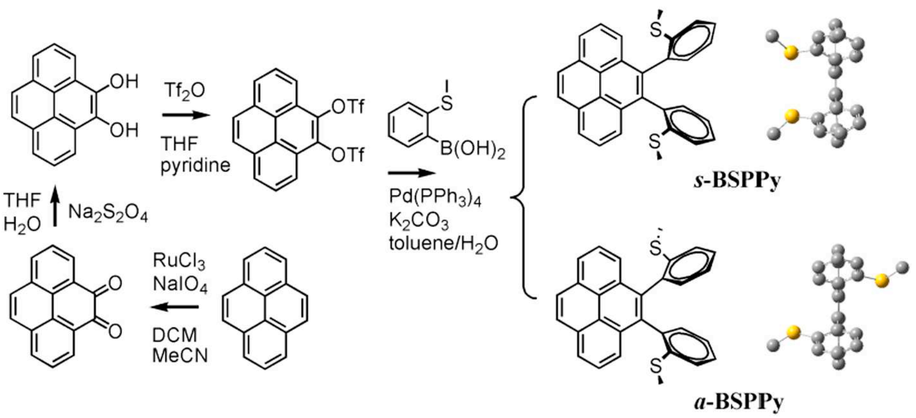

Scheme 1. Synthesis route for ***s*-BSPPy** and ***a*-BSPPy.**

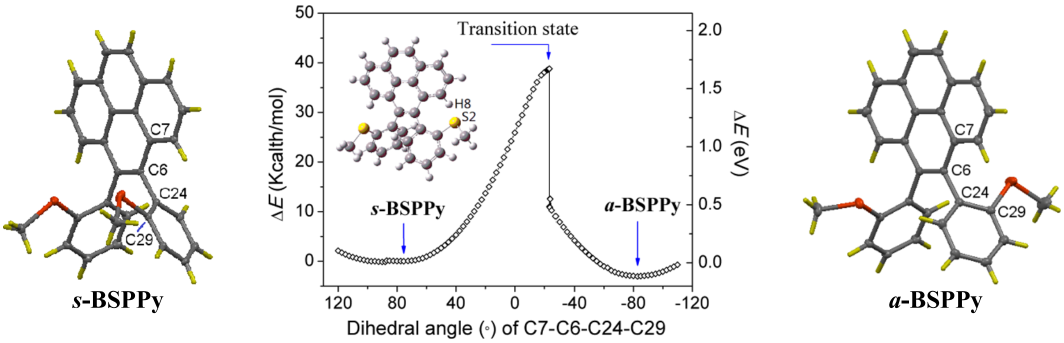

Fig. 1. The potential energy curve for series of relaxed conformations transforming from ***s*-BSPPy** to ***a*-BSPPy**, calculated by series of optimizations with series of the C7-C6-C24-C29 dihedral angles being "frozen" in every course of optimization. The energy of the transition state is 38.8 kcalth/mol higher than that of ***s*-BSPPy**.

arise from hindered rotation about a single bond, where the rotation energy barrier is high enough to prevent interconversion from one conformer to another and therefore individual conformers can be isolated [16]. Various enantioseparation techniques have to be developed to separate atropisomers [17,18], while ***s*-BSPPy** and ***a*-BSPPy** can be separated by simple silica gel chromatography (see Fig. S1 in Supplementary Information (SI)). The X-ray structural analyses confirmed that the two *S*-methyl groups are on the same side of the pyrene plane for ***s*-BSPPy** (*syn*-isomer, see Fig. 1), but on the opposite side of the pyrene plane for ***a*-BSPPy** (*anti*-isomer, see Fig. 1). Herein, we mainly report the different excimer-monomer emission properties and the Ag^+-response behaviors of ***s*-BSPPy** and ***a*-BSPPy**.

The synthetic route for ***s*-BSPPy** and ***a*-BSPPy** is shown in Scheme 1 (see SI for detailed syntheses). IR spectra were recorded with KBr pellets on a Thermo Nicolet Avatar 370 FTIR spectrometer. UV–vis absorption spectra were obtained with a Shimadzu UV-2550 spectrophotometer. Fluorescence spectra were recorded on an Edinburgh FLS920 fluorescence spectrometer. The quantum chemistry calculations, including the geometric optimizations, energies, vibration frequencies, dipole moments, and the electronic transfer integrals, were carried out within the framework of DFT/B3LYP/6-311 g(d) by using Gaussian 09 programs [19].

Single crystals of ***s*-BSPPy** and ***a*-BSPPy** were grown from their petroleum ether/DCM solutions and their X-ray diffraction data were collected by a Bruker APEX-II diffractometer (Mo-*Kα* radiation) at 100 K. The structures were resolved and refined by the APEX-II and SHELXL-2014 programs. All the atomic ellipsoids of the X-ray molecular structures (in Figs. 1 and 4) were drawn at the 50% probability level.

***s*-BSPPy** crystal belongs to $P2_1/c$ space group; a, b, c = 8.9475(4), 9.6550(5), 25.1433(13) Å; β = 92.6613(9)°; V = 2169.74(19) $Å^3$; $\rho = 1.367\ g/cm^3$; M.P. = 270–271 °C. The refinement converged to: $R_1 = 0.0328$. ***a*-BSPPy** crystal belongs to $P2_1/n$ space group; a, b, c = 12.1277(3), 15.7933(4), 12.2777(3) Å; β = 106.9550(10)°; V = 2249.41(10) $Å^3$; $\rho = 1.319\ g/cm^3$; M.P. = 227–228 °C. The refinement converged to: $R_1 = 0.0389$. The detailed crystalline and refraction data can be found in Table S1 in SI.

The geometry of ***a*-BSPPy** can be optimized to the C_2 point group, while the proximately C_s symmetric ***s*-BSPPy** strictly belongs to the C_1 point group. The calculated total energy of ***a*-BSPPy** molecule is slightly (0.132 eV) lower than that of ***s*-BSPPy** (shown in Fig. 1), however ***s*-BSPPy** crystal is more stable for its more tightly packing (higher density) and higher melting point.

Many simple methods can differentiate ***s*-BSPPy** and ***a*-BSPPy**, such as NMR (Fig. S2 in SI), IR (Fig. S3 in SI), and thin layer chromatography (Fig. S1 in SI). The calculated dipole moment of ***a*-BSPPy** (2.14 Debye) is smaller than that of ***s*-BSPPy** (2.54 Debye), which is consistent with their chromatographic sequence (see Fig. S1). As shown in the IR spectra in Fig. S3, the characteristic peak at 864 cm^{-1} of ***s*-BSPPy** is strong while that of ***a*-BSPPy** is very weak. This peak can be assigned to the out-of-plane C—H bending vibration of the phenyl group (see Fig. S4 in SI).

As shown in Fig. 1, the height of the calculated rotation barrier (rotating around the C6—C24 bond to transform ***s*-BSPPy** to ***a*-BSPPy**) is 38.8 kcalth/mol, which is two orders of magnitude higher than the thermal energy k_BT = 0.596 kcalth/mol at 300 K. The main hindrance from rotation may be the intense S2…H8 (2.312 Å) steric repulsion at the transition state (see the inset of Fig. 1), which makes the pyrene plane slightly curved. The high rotation barrier can well interpret the fact that both atropisomers ***s*-BSPPy** and ***a*-BSPPy** are conformational stable and no trace of interconversion was observed after refluxing in toluene for 24 h.

The absorption spectra (shown in Fig. S5) of ***s*-BSPPy** and ***a*-BSPPy** are quite similar with actually the same peak wavelengths, while the

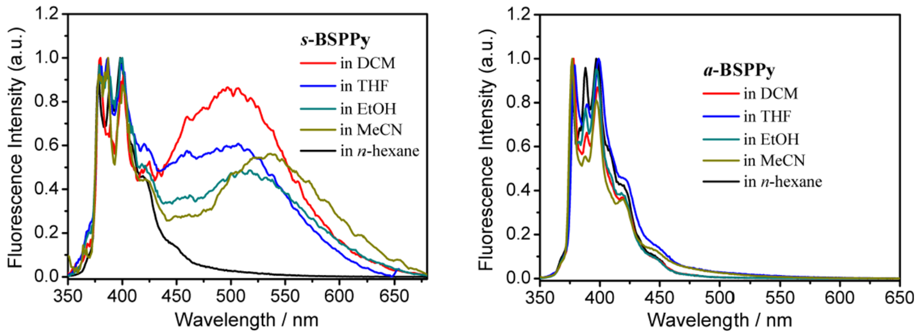

(a)

(b)

Fig. 2. Normalized fluorescence spectra (λ_{ex} = 345 nm, c = 28 μM) of (a) ***s*-BSPPy** and (b) ***a*-BSPPy** in various solvents. For ***s*-BSPPy**, the ratios ($I_{excimer}/I_{monomer}$) in DCM (I_{503}/I_{400}), THF (I_{503}/I_{399}), EtOH (I_{512}/I_{400}), MeCN (I_{531}/I_{400}) are 0.97, 0.63, 0.49, 0.65, respectively. Emission quantum yields of ***s*-BSPPy** and ***a*-BSPPy** were determined to be 0.3% and 2.6%, respectively, in EtOH using anthracene (Φ = 28%) as reference.

molar absorption coefficient (ε) of ***s*-BSPPy** is larger than that of ***a*-BSPPy** in both DCM and MeCN.

As shown in Fig. 2a, ***s*-BSPPy** shows a monomeric emission characterized by the longest peak wavelength at 398 nm in *n*-hexane, which is similar to that of ***a*-BSPPy** (397 nm in *n*-hexane). In polar solvents, a new broad peak at longer wavelength, 503 nm in DCM and red-shifted to 531 nm in MeCN, appears in the emission spectra of ***s*-BSPPy**, which is the feature of the excimer emission (Fig. 2a). However, no excimer-emission of ***a*-BSPPy** was observed in the same solvents (see Fig. 2b).

The concentration-dependent fluorescence spectra of ***s*-BSPPy** and ***a*-BSPPy** in DCM are shown in Fig. 3. The ratio of I_{503}/I_{400} increases with increasing the concentration of ***s*-BSPPy** (Fig. 3a), indicating that the excimer of ***s*-BSPPy** is intermolecular type, not intramolecular kind. Meanwhile no excimer emission of ***a*-BSPPy** can be observed at any concentration (Fig. 3b).

To figure out the excimer model of the ***s*-BSPPy**, the intermolecular interactions between two neighboring molecules (two-molecule pair) are considered and can be scaled by the electronic transfer integral, *t*, of the concerned molecular pair. The *t* value can be approached by following Eq. [20].

$$t = \frac{1}{2}(E_{\mathrm{HOMO}} - E_{\mathrm{HOMO-1}}) \tag{1}$$

where E_{HOMO} and $E_{\mathrm{HOMO\text{-}1}}$ are the energy levels of the HOMO and HOMO-1 of a two-molecule pair, respectively. All the geometries of the concerned molecular pairs for the *t*-calculations are based on the X-ray structures without optimization.

As shown in Fig. 4a, there are four molecules (II, III, IV, V) [I: (x, y, z); II: (1-*x*, 0.5 + y, 1.5-z); III: (1-*x*, −0.5 + y, 1.5-z); IV: (1-*x*, 1-y, 1-z); V: (1-*x*, −y, 1-z)] around the central molecule I in ***s*-BSPPy** crystal. The calculated *t* values, corresponding to molecular pairs (I–II), (I–III), (I–IV), and (I–V) show a sequence of

$$t_{\mathrm{I,V}}\ (3.\ 5\ \mathrm{meV}),\ \ t_{\mathrm{I,IV}}\ (21\ \mathrm{meV}) < < t_{\mathrm{I,III}}\ (67\ \mathrm{meV}) \approx t_{\mathrm{I,II}}\ (68\ \mathrm{meV}).$$

The $t_{\mathrm{I,\ IV}}$ and $t_{\mathrm{I,V}}$ are trivial and there are no short contacts between the two pyrene moieties of the I–IV or I–V pairs, though there is a short S2…S2(IV) contact of 3.2595(4) Å between I and IV and a weak hydrogen bond of C27-H27…S1(V) (see Table S3 in SI) between I and V. Thus the possibility of molecular pairs (I–IV) or (I–V) being the excimer can be excluded. The dimer of (I–II) or (I–III) takes a kind of edge-to-face λ-shaped conformation and may play the role of excimer, for the $t_{\mathrm{I,II}}$ and $t_{\mathrm{I,III}}$ values are considerable large. The large *t* value of the I–II or I–III can be attributed to the C-H…π (II or III) as well as the C-H…C (II or III) interactions (listed in Table S3 in SI). Taking the I-II pair for example, the distances of H12 and H13 to the pyrene plane of II are 2.660(16) and 2.672(17) Å respectively, much shorter than the van der Waals H…π distance of 3.0 Å. The molecules I and II (I and III as well) are non-parallel oriented with a dihedral angle of 56.5° between their two pyrene planes (see Fig. 4b). By the C-H…π and C-H…C interactions, a kind of one dimensional zigzag chain has been constructed along the *b*-axis direction, in which the adjacent two molecules of the λ-shaped edge-to-face pair are related each other by 2_1 screw operation (see Fig. 4b).

It is well-established that the excited-state dimer (excimer) of the pyrene compounds commonly takes a parallel face-to-face π…π geometry. Recently, the non-parallel T-shaped excimer [21] and the tilt-slide-shaped excimer [22] of anthracene compounds have been reported. A tweezer type of pyrene compound, with its two pyrene subunits being non-parallel oriented, has been reported to display intramolecular excimer emission [23]. Pyrene derivatives with non-parallel "herringbone" packing style have also been reported to exhibit intermolecular "excimer-like" emission [24]. These examples provided, to a certain extent, some supports to the supposed non-parallel edge-to-face λ-shaped conformation of the ***s*-BSPPy** excimer.

In recent years, chelatable-S-containing sensors have been designed to detect various metal ions, such as Ni^{2+} [25], Hg^{2+} [26], Ag^{+} [26]. Now that there are two chelatable S atoms in ***s*-BSPPy,** the selective

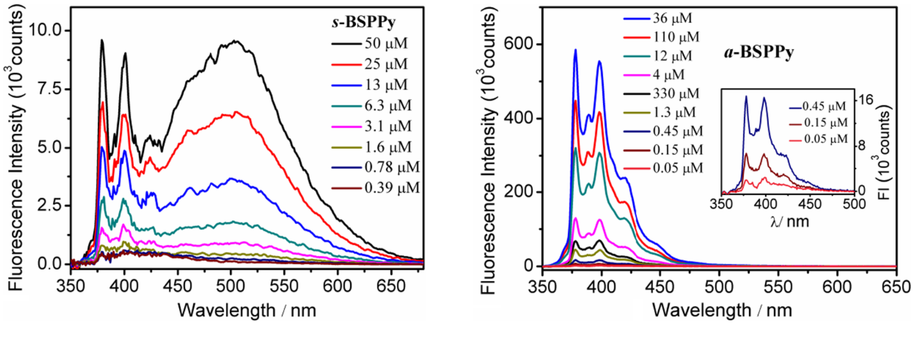

(a)

(b)

Fig. 3. Fluorescence spectra (λ_{ex} = 345 nm) of (a) ***s*-BSPPy** and (b) ***a*-BSPPy** in various concentrations in DCM. For ***s*-BSPPy**, the ratios (I_{503}/I_{400}) in concentration of 50, 25, 13, 6.3, 3.1, 1.6, 0.78, 0.39 μM are 1.06, 1.01, 0.73, 0.68, 0.51, 0.46, 0.38, 0.25, respectively.

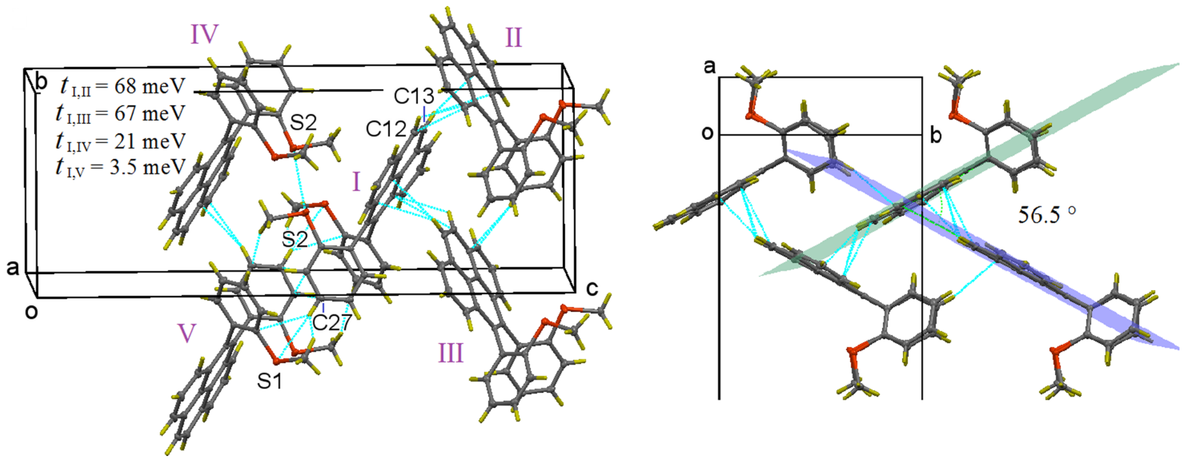

(a) (b)

Fig. 4. X-ray structure (T = 100 K) of single-crystal ***s*-BSPPy**. (a) A view along the *a*-axis, showing the central molecule (I) and its adjacent molecules (II, III, IV, V) with the *t* values being indicated. (b) The 1-D chain along the *b*-axis with a dihedral angle between the two mean planes of the two pyrene moieties being indicated.

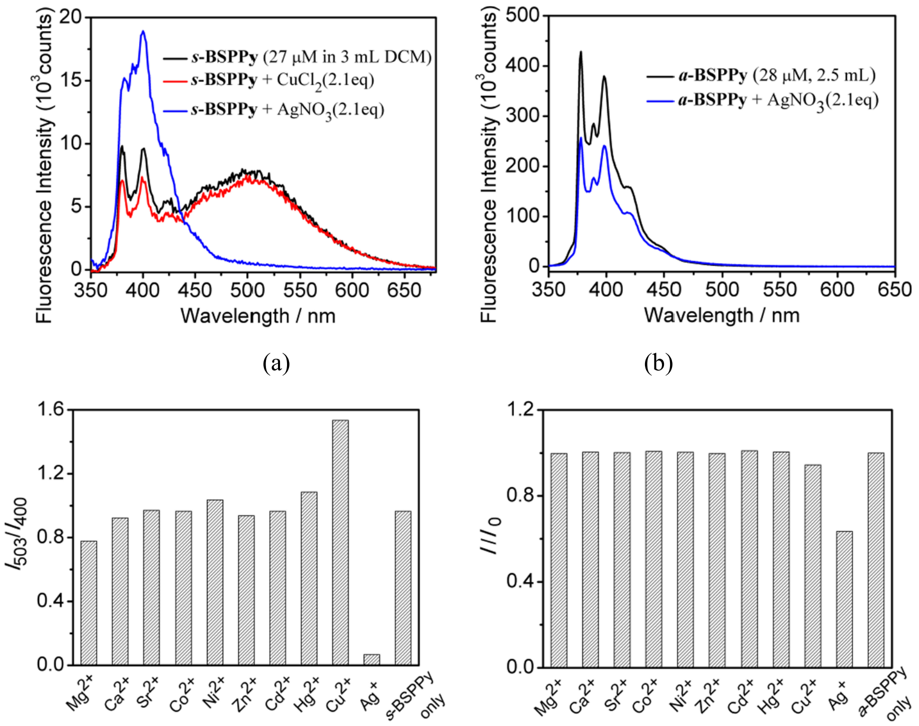

(a) (b)

(c) (d)

Fig. 5. (a) (b) Fluorescence spectra of ***s*-BSPPy** and ***a*-BSPPy** (λ_{ex} = 345 nm) in DCM upon addition of 2.1 equiv. of $CuCl_2$ or $AgNO_3$ (15 mM in 10 μL EtOH, respectively). (c) Metal ions (chlorizated salts of Sr^{2+}, Co^{2+}, Ni^{2+}, Hg^{2+}, Cu^{2+}; acetate salts of Zn^{2+}, Cd^{2+}; nitrate salts of Mg^{2+}, Ca^{2+}, Ag^{+}) selectivity of ***s*-BSPPy** in 27 μM DCM solutions. The emission intensity ratios (I_{503}/I_{400}) of ***s*-BSPPy** + M^{n+}/DCM solutions are 0.97(Sr^{2+}), 0.96(Co^{2+}), 1.04(Ni^{2+}), 1.08(Hg^{2+}), 1.53(Cu^{2+}), 0.94(Zn^{2+}), 0.96(Cd^{2+}), 0.78(Mg^{2+}), 0.92(Ca^{2+}), 0.067(Ag^{+}). (d) Metal ions selectivity of ***a*-BSPPy** in 28 μM DCM. I_0 and I denote the fluorescence intensity of ***a*-BSPPy** and ***a*-BSPPy** + M^{n+} at 398 nm.

fluoroionophoric behavior of ***s*-BSPPy** to various cations has been investigated. As presented in Fig. 5a, 2.1 equiv $AgNO_3$ completely quenched the excimer emission and greatly enhanced the monomer emission of ***s*-BSPPy** in DCM solution, while no significant fluorescence changes can be observed upon adding same amounts of other metal ions (Fig. 5c). For ***a*-BSPPy**, only a moderate reduction of the monomer emission has been observed, which was uniquely induced by Ag^+ (see Fig. 5b and d). In comparison with ***a*-BSPPy**, the Ag^+-response of ***s*-BSPPy** is more interesting because of its remarkable ratiometric excimer-to-monomer emission [27,28].

As shown in Fig. 6a, the fluorescence titration spectra of ***s*-BSPPy** with Ag^+ exhibits a stepwise decrease of the excimer emission (turn-off) and a concomitant enhancement of the monomer emission (turn-on) with an isoemission point at 438 nm. This off-and-on evolution of the titration spectra tends to saturation when the Ag^+ amounted to 2.1 equiv. In the course of titration, the ratio of emission intensities (I_{503}/I_{400}) underwent a dramatic change from 0.96 to 0.067, demonstrating the potential application of ***s*-BSPPy** as a ratiometric chemosensor for Ag^+.

In addition, competition experiment was performed to check the Ag^+-selectivity of ***s*-BSPPy** in the presence of Ag^+ and other metal ions (Fig. 6b). The addition of other competition ions to the ***s*-BSPPy**/DCM solution did not make obvious changes to the emission spectra. Upon further adding Ag^+ to the above ***s*-BSPPy** + M^{2+}/DCM system, great changes of the I_{503}/I_{400} ratio took place. Therefore, ***s*-BSPPy** may be used as a Ag^+-selective chemodosimeter. The excimer-emission-off and monomer-emission-on behavior of ***s*-BSPPy** in the presence of Ag^+ can be attributed to the chelation of the S atoms to the Ag^+ ion.

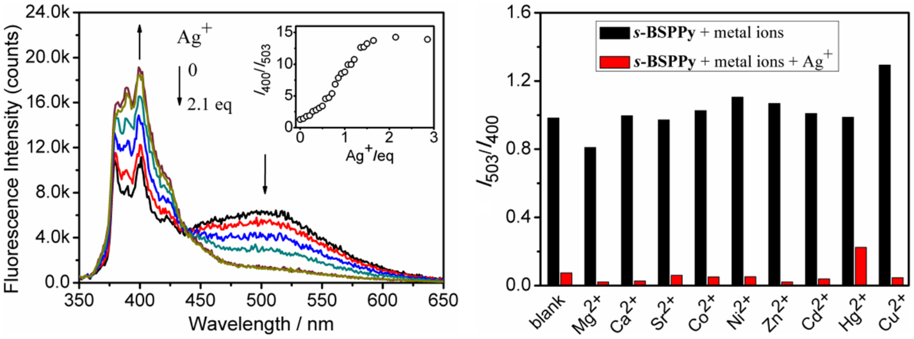

(a) (b)

Fig. 6. (a) Fluorescence spectra of **_s_-BSPPy** (λ_{ex} = 345 nm, c = 28 μM, 2.5 mL DCM) upon stepwise adding a total of 2.1 equiv. of $AgNO_3$ (1 mM in EtOH). Inset: Ratiometric fluorescence intensity I_{400}/I_{503} as a function of the amount of Ag^+. (b) Competition experiments: fluorescence intensity ratio I_{503}/I_{400} of series of host solutions of **_s_-BSPPy** (c = 28 μM, 2.5 mL DCM), containing 2.1 equiv. of guest ions (15 mM in 10 μL EtOH) of Ag^+ and separately, 2.1 equiv of other metal ions.

In summary, the monomer-excimer emission properties of the **_s_-BSPPy** and **_a_-BSPPy** atropisomers have been carefully investigated. In comparison with **_a_-BSPPy**, **_s_-BSPPy** features non-parallel λ-shaped geometry of the excimer and exhibits interesting emission properties, such as (1) monomer-excimer emission in polar solvents; (2) the unique ratiometric Ag^+ response of the on-and-off kind of the monomer-and-excimer emission. To our knowledge, the monomer-excimer emission properties of the pyrene derivatives, which are originated from the λ-shaped intermolecular-dimer and can be regulated by Ag^+ ion, have not been previously reported.

Acknowledgments

This work was supported by the National Natural Science Foundation of China (Grant nos. 21472116, 21871165, and 21672130) and the State Key Laboratory of Crystal Materials.

Appendix A. Supplementary material

Cambridge Crystallographic Data Centre (CCDC) contain the crystallographic information files (CIF) for this paper, numbered 1,564,521 (**_s_-BSPPy** at 100 K), 1,564,533 (**_a_-BSPPy** at 100 K). These data can be obtained free of charge from CCDC via www.ccdc.cam.ac.uk/data_request/cif. The experimental details, Figures of thin-layer chromatogram, ^{1}H NMR spectra, IR spectra, Tables of X-ray crystallography data, and the UV–vis absorption spectra can be found in the SI. Supplementary material to this article can be found online at https://doi.org/10.1016/j.inoche.2018.12.021.

References

[1] J.B. Birks, Photophysics of Aromatic Molecules, John Wiley, New York, 1970.
[2] F.M. Winnik, Photophysics of preassociated pyrenes in aqueous polymer solutions and in other organized media, Chem. Rev. 93 (1993) 587–614.
[3] T.M. Figueira-Duarte, K. Müllen, Pyrene-based materials for organic electronics, Chem. Rev. 111 (2011) 7260–7314.
[4] J. Feng, L. Xiong, S. Wang, S. Li, Y. Li, G. Yang, Fluorescent temperature sensing using triarylboron compounds and microcapsules for detection of a wide temperature range on the micro- and macroscale, Adv. Funct. Mater. 23 (2013) 340–345.
[5] L. Ji, R.M. Edkins, A. Lorbach, I. Krummenacher, C. Brückner, A. Eichhorn, H. Braunschweig, B. Engels, P.J. Low, T.B. Marder, Electron delocalization in reduced forms of 2-(BMes$_2$)pyrene and 2,7-Bis(BMes$_2$)pyrene, J. Am. Chem. Soc. 137 (2015) 6750–6753.
[6] S. Zhang, Z. Liu, Q. Fang, Synthesis, structures, and optoelectronic properties of pyrene-fused thioxanthenes, Org. Lett. 19 (2017) 1382–1385.
[7] K.-H. Chu, Y. Zhou, Y. Fang, L.-H. Wang, J.-Y. Li, C. Yao, Rhodamine-pyrene conjugated chemosensors for ratiometric detection of Hg^{2+} ions: different sensing behavior between a spirolactone and a spirothiolactone, Dyes Pigments 98 (2013) 339–346.
[8] Y.H. Lee, M.H. Lee, J.F. Zhang, J.S. Kim, Pyrene excimer-based calix[4]arene FRET chemosensor for mercury(II), J. Org. Chem. 75 (2010) 7159–7165.
[9] Y. Zhou, C.-Y. Zhu, X.-S. Gao, X.-Y. You, C. Yao, Hg^{2+}-selective ratiometric and “off-on” chemosensor based on the azadiene-pyrene derivative, Org. Lett. 12 (2010) 2566–2569.
[10] H. Xie, Y. Wu, J. Huang, F. Zeng, H. Wu, X. Xia, C. Yu, S. Wu, A ratiometric fluorescent probe for aluminum ions based-on monomer/excimer conversion and its applications to real samples, Talanta 151 (2016) 8–13.
[11] J.-L. Zhao, H. Tomiyasu, C. Wu, H. Cong, X. Zeng, S. Rahman, P.E. Georghiou, D.L. Hughes, C. Redshaw, T. Yamato, Synthesis, crystal structure and complexation behaviour study of an efficient Cu^{2+} ratiometric fluorescent chemosensor based on thiacalix[4]arene, Tetrahedron 71 (2015) 8521–8527.
[12] X.-L. Ni, S. Wang, X. Zeng, Z. Tao, T. Yamato, Pyrene-linked triazole-modified homooxacalix[3]arene: a unique C3 symmetry ratiometric fluorescent chemosensor for Pb^{2+}, Org. Lett. 13 (2010) 552–555.
[13] L. Gai, H. Chen, B. Zou, H. Lu, G. Lai, Z. Li, Z. Shen, Ratiometric fluorescence chemodosimeters for fluoride anion based on pyrene excimer/monomer transformation, Chem. Commun. 48 (2012) 10721–10723.
[14] B. Schazmann, N. Alhashimy, D. Diamond, Chloride selective calix[4]arene optical sensor combining urea functionality with pyrene excimer transduction, J. Am. Chem. Soc. 128 (2006) 8607–8614.
[15] Y. Wu, J. Wang, F. Zeng, S. Huang, J. Huang, H. Xie, C. Yu, S. Wu, Pyrene derivative emitting red or near-infrared light with monomer/excimer conversion and its application to ratiometric detection of hypochlorite, ACS Appl. Mater. Interfaces 8 (2016) 1511–1519.
[16] G. Bringmann, A.J.P. Mortimer, P.A. Keller, M.J. Gresser, J. Garner, M. Breuning, Atroposelective synthesis of axially chiral biaryl compounds, Angew. Chem. Int. Ed. 44 (2005) 5384–5427.
[17] P. Peluso, V. Mamane, E. Aubert, S. Cossu, Recent trends and applications in liquid-phase chromatography enantioseparation of atropisomers, Electrophoresis 00 (2017) 1–21.
[18] K. Wu, K. Li, Y.-J. Hou, M. Pan, L.-Y. Zhang, L. Chen, C.-Y. Su, Homochiral D_4-symmetric metal-organic cages from stereogenic Ru(II) metalloligands for effective enantioseparation of atropisomeric molecules, Nat. Commun. 7 (2016) 10487–10496.
[19] M.J. Frisch, et al., Gaussian 09, Gaussian, Inc., Wallingford, CT, 2010.
[20] W.-Q. Deng, W.A. Goddard III, Predictions of hole mobilities in oligoacene organic semiconductors from quantum mechanical calculations, J. Phys. Chem. B 108 (2004) 8614–8621.
[21] G. Zhang, G. Yang, S. Wang, Q. Chen, J.S. Ma, A highly fluorescent anthracene-containing hybrid material exhibiting tunable blue-green emission based on the formation of an unusual “T-shaped” excimer, Chem. Eur. J. 13 (2007) 3630–3635.
[22] M. Sugino, Y. Araki, K. Hatanaka, I. Hisaki, M. Miyata, N. Tohnai, Elucidation of anthracene arrangement for excimer emission at ambient conditions, Cryst. Growth Des. 13 (2013) 4986–4992.
[23] S.K. Kim, J.M. Lim, T. Pradhan, H.S. Jung, V.M. Lynch, J.S. Kim, D. Kim, J.L. Sessler, Self-association and nitroaromatic-induced deaggregation of pyrene substituted pyridine amides, J. Am. Chem. Soc. 136 (2014) 495–505.
[24] S.K. Rajagopal, A.M. Philip, K. Nagarajan, M. Hariharan, Progressive acylation of pyrene engineers solid state packing and colour *via* C–H…H–C, C–H…O and π − π interactions, Chem. Commun. 50 (2014) 8644–8647.
[25] A. Banerjee, A. Sahana, S. Guha, S. Lohar, I. Hauli, S.K. Mukhopadhyay, J.S. Matalobos, D. Das, Nickel(II)-induced excimer formation of a naphthalene-based fluorescent probe for living cell imaging, Inorg. Chem. 51 (2012) 5699–5704.
[26] Y. Hiruta, H. Koiso, H. Ozawa, H. Sato, K. Hamada, S. Yabushita, D. Citterio, K. Suzuki, Near IR emitting red-shifting ratiometric fluorophores based on borondipyrromethene, Org. Lett. 17 (2015) 3022–3025.
[27] F. Wang, R. Nandhakumar, J.H. Moon, K.M. Kim, J.Y. Lee, J. Yoon, Ratiometric fluorescent chemosensor for silver ion at physiological pH, Inorg. Chem. 50 (2011) 2240–2245.
[28] L. Liu, D. Zhang, G. Zhang, J. Xiang, D. Zhu, Highly selective ratiometric fluorescence determination of Ag^+ based on a molecular motif with one pyrene and two adenine moieties, Org. Lett. 10 (2008) 2271–2274.